Kufa Journal of Engineering
Vol. 14, No. 4, October 2023, P.P. 69-85
Article history: Received date: 15 September 2023, accepted date: 12 October 2023

PERFORMANCE EVALUATION OF HOT AIR THERMOELECTRIC GENERATOR USING BIOMASS ENERGY SOURCE

Francis Onoroh[1], Mercy Ogbonnaya[2] and Larry Orobome Agberegha[3]

1 Department of Mechanical Engineering, University of Lagos, Akoka, Lagos, Nigeria. Email: fonoroh@unilag.edu.ng

2 Department of Mechanical Engineering, University of Lagos, Akoka, Lagos, Nigeria. Email: mogbonnaya@unilag.edu.ng

3 Department of Mechanical Engineering, Federal University of Petroleum Resources, Delta state, Nigeria. Email: agberegha.larry@fupre.edu.ng

HTTPS://DOI.ORG/10.30572/2018/KJE/140406

ABSTRACT

Thermoelectric generators are solid-state devices that convert heat into electricity using the Seebeck effect, when there is a temperature difference across a thermoelectric material. This research designed an experimentally tested a thermoelectric hot air generator using sixteen SP1848-27145 modules in two parallel strings. The system consists of a biomass combustion chamber, hot air exhauster, hot and cold side heat exchangers. Voltage, current and temperatures in the combustion chamber, hot air heat exhauster, hot side heat exchanger and cold side heat sink were measured. The hot air exhauster, hot side heat sink and cold side maximum temperatures are 178.3°C, 69.2°C and 44.5°C respectively yielding an open circuit voltage of 64 V and current of 1.99 A in the course of the experiment. The thermal performance of the designed hot air exhauster, hot side heat exchanger and cold side heat were simulated using ANSYS Fluent, for pictorial representation of their temperature contours.

KEYWORDS: Hot air; Temperature; Exhauster; Biomass; Modules; Combustion.

Article information: This manuscript was handled by Abbas Al-Hdabi, Managing Editor.

1. INTRODUCTION

Electricity is a key part of life and hence almost impossible to live without. We depend heavily on electricity in our daily activities. Our everyday routines heavily rely on the use of energy, whether it be at home, school, the neighborhood retail mall, or our place of employment. (Zohuri, 2016). Compared to other energy sources, electricity has a number of advantages, including the ability to power much more efficient lighting, information and communication systems, and more efficient manufacturing processes. The ability to provide consistent power to everyone in the world has come a long way in recent years, but some areas continue to be particularly underserved. For development organizations and governments to justify their intervention to expand access to and reliability of electricity, it is desirable to know that the intervention would have a causal influence on economic growth, poverty, and other crucial development indicators (Stern et al., 2019). Traditional thermal power plants will increase the amount of pollutants and carbon dioxide released into the atmosphere when they produce energy, which is contrary to what is required in a sustainable society. Promoting clean energy power generation, particularly renewable energy generation, appears to be a logical decision given the demands of increasing energy demand and the goal of reducing carbon emissions (Wang and Li, 2021). Burning fossil fuel contribute to global warming, ozone depletion and unreliable supply, hence the need for more effective power generation system.

Solar energy became a very vital way to generate electricity. Solar technologies help to generate electricity by trapping sunlight via photovoltaic panels known as solar panels or by using mirrors, earth receives sunlight above 1366 W daily (Shaikh et al., 2017). This technology provides electricity from renewable energy source which makes it so important and sustainable. This energy source is completely free and endlessly usable. The main benefit of solar energy over other conventional power sources is that it can be generated using the smallest photovoltaic (PV) solar cells, allowing sunlight to be converted directly into solar energy. A lot of study has been done to combine the sun's energy process by creating solar cells, panels and modules with high converting efficiency (Saraswathi, 2020). This means of electricity generation has some limitations; in areas with very low sunlight, cloudy and raining days, solar irradiation is very poor and totally absent at night. Due to the need to improve and ensure constant supply of electricity in scenarios like this, another means of electricity became apparent. Thermoelectric generators (TEGs) are solid-state devices that exploit the Seebeck effect, a process that results in voltage generation when there is a temperature difference across a thermoelectric material, to convert waste heat and cheap and readily available into electrical power (Zhu et al, 2014).

Generation of electricity from hot air become a perfect aid to sunlight. In this technology a device called thermoelectric module helps to convert heat energy directly into electrical energy. The heat can be generated from diverse sources, gas, coal, charcoal, etc. The air in the heat exchanger gets heated up by combustion of fuel in the combustion chamber and moves through several passes to ensure the air is well heated up to the required temperature which in turns heats up the thermoelectric modules and in turn generate electricity. Hot air thermoelectric power generation is not restricted to weather condition and it can be operated at any time of the day. The need to addressing energy poverty in the development debate is strongly supported by the highly important magnitude of electricity's impact on quality of life (Bridge, 2016).

Using the finite element program ANSYS, Virjoghe et al. (2018) worked on the numerical simulation of thermoelectric systems. Preprocessor, solver, and postprocessor are the three stages in which the package operates. Using PREP 7, a physics environment was constructed, a model was developed, meshed, and physics characteristics were assigned to each part of the model. After applying boundary conditions, the solution was run, and the results were reviewed. They came to the conclusion that a lower electrical resistivity will result in less Joule heating, a lower thermal conductivity will result in less heat transfer between the modules, and a higher Seebeck or Peltier coefficient will result in a faster rate of heat removal.

Using a solar concentrator, Fresnel lens, reflecting materials, and solar tracking as a source of heat and a heat sink for heat dissipation, Binu et al. (2017) designed and created a thermoelectric power generator. The Fresnel lens was used to obtain high concentration of solar energy, an inverter was used to convert DC voltage to AC voltage. Their finding indicates the thermoelectric generator performance indices of current, voltage and power is optimal with a hot and cold side temperatures of final maximum output 300°C and cold side 100°C.

Ong (2016) examined thermoelectric hybrid systems, heat pipes, and solar energy for electrical and heating purposes. Heat was dissipated by coolant water flowing in the condenser manifold. The thermal efficiency of a solar, heat pipe, and thermoelectric hybrid system was determined to be comparable to and not significantly lower than that attained with the current application of an Evacuated Tube Heat Pipe Solar Collector (ETHPSC). He came to the conclusion that a solar heat pipe collector with thermoelectric modules could be a very practical tool for generating power and heating water at the same time. Small, portable, moveable, and off-grid power and heating systems could be provided by such hybrid systems for home or small-scale industrial purposes.

Remeli et al. (2015) designed a thermoelectric generator and heat pipe that used a counter-flow air duct heat exchanger to generate power from waste heat. Eight thermoelectric modules sandwiched between two copper blocks were intended to fit within the set-up. A copper coil heater with a temperature setting of 108°C supplied the heat source. The outcome of the experiment demonstrates that improving the mass flow rate in the higher duct relative to the lower duct improves system performance as a whole. Power production and heat transfer are both increased by a larger mass flow rate ratio.

The comparative evaluation of thermoelectric generator energy generation was the focus of Stecanella et al. (2015) investigation. A stainless steel device with a 5mm thickness and a hexagonal shape was put in the generator's exhaust duct. The hot side of the thermoelectric generators receives heat transfer through conduction from the exhaust gases of the electric generators. An electronic device called a programmable logic controller continuously measures the hot and cold temperatures of thermoelectric generators. According to the results, the critical point's temperatures are 350°C on the hot side and 30°C on the cold side, with a heat flow of 247 W and an electric power output of 21.7 W, respectively.

From the review of literature, various works have been done on thermoelectric power generation. Most of these centered on using solar as the energy source and it is known that its reliability cannot be completely guaranteed due to the dynamic nature of weather conditions. At night, there is usually little or no sunshine which reduces its effectiveness. Biomass on the other hand is readily available and can be deployed at any time of the day irrespective of prevailing weather condition. Thus, this research focused on the design of a unique hot air thermoelectric generator consisting of a combustion chamber, hot air exhaust chamber, hot side heat exchanger and cold side heat sink. The hot air exhaust chamber absorbs energy during combustion and the exhaust hot air serves as the energy source for the thermoelectric modules to prevent them from excessive combustion temperature that could lead to thermal induced failure. Practical application areas include battery charging stations, off grid centers, rural communities and even in city centers due to the high cost of electricity tariffs and rising cost of petroleum products in internal combustion engine generators.

2. GENERATOR ARCHITECTURE

The model of the generator and its exploded as shown in Fig. 1 consist of the hot side multi pass heat exchanger and cold side heat sink with cooling fans, thermoelectric modules sandwiched in between, the hot air extractor a dual combustion.

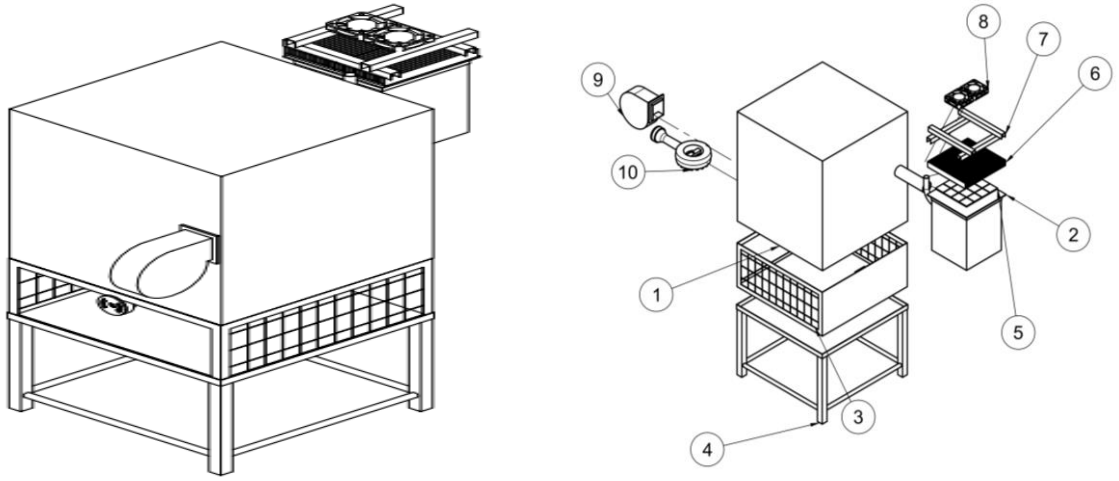

Parts: 1. Hot air exhauster 2. Hot side heat exchanger 3. Combustion chamber 4. Stand 5. Thermoelectric module 6. Cold side heat exchanger 7. Cooling fan stand 8. Fans 9. Blower 10. Gas burner

Fig. 1. Model of Hot Air Thermoelectric Generator.

2.1. Combustion Chamber

The combustion chamber is rectangular and perforated to ensure that there is sufficient air for combustion. It is a dual combustion chamber either charcoal and natural gas can be used as fuel, with a provision for easy dismantling of the gas burner if charcoal is to be burn. The design specification is such that the combustion hot air heat exhauster has a thermal storage steel plate to be maintained at a minimum temperature of 1000°C. The constructional details of the combustion chamber is as shown in Fig. 2.

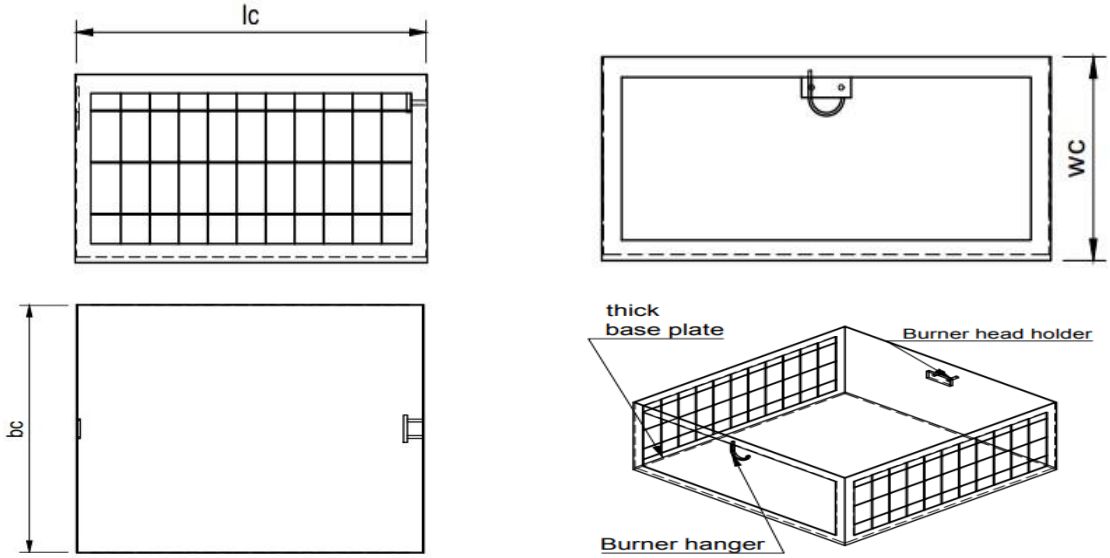

Dimensions in mm: $Ic = bc = 450, Wc = 200$

Fig. 2. Combustion Chamber.

2.2. Hot Air Exhaust Chamber

A heat exchanger ensures efficient heat transfer from one medium to another and the constructional features can be tailored to specific process design (Nimankar and Dahake, 2016; Reyes-León et al, 2011). The exhauster is a heat exchanger with five air passes to ensure the air absorb maximum amount of heat during the combusting process as the air is expected to exit the exhauster at a minimum temperature of 100°C. The constructional details of the hot air exhauster is as shown in Fig. 3. The heat capacity of the inlet and outlet air are expressed as equation (1) and (2) respectively (Çengel et al, 2022):

$$C_i = \dot{m}_\iota \times C_{pi} \quad (1)$$

$$C_o = \dot{m}_o \times C_{po} \quad (2)$$

Where $\dot{m}_\iota$ and $\dot{m}_o$ are the mass flow rate of inlet and outlet air supplied by the blower, kgs^{-1}; C_{pi} and C_{po} are the specific heat capacity of inlet and outlet air $kJkg^{-1}K^{-1}$. For steady flow:

$$\dot{m}_\iota = \dot{m}_o$$

The heat absorbed by air due to combustion in the combustion chamber is determined using equation (3):

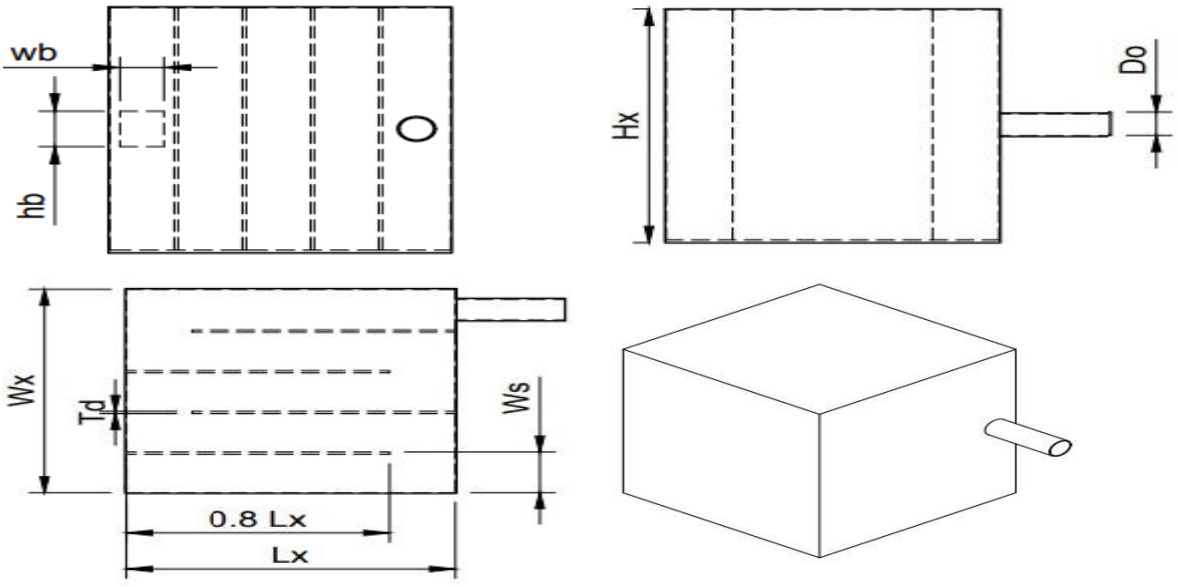

Dimensions in mm: $Hx = 500, Do = 45, Wx = 450, Ws = 90, Lx = 450, Td = 5, Wb = 58, hb = 72$

Fig. 3. Combustion Hot air exhauster

$$Q_a = C_c \times (T_e - T_a) \quad (3)$$

$$C_c = C_i \; if \; C_i < C_o \quad (4)$$

$$C_c = C_o \; if \; C_i > C_o \quad (5)$$

Where T_e is the exit temperature of air from the exhauster, K; and T_a is the ambient temperature, K. The maximum possible heat to be absorbed by the air is obtained using equation (6):

$$Q_{ma} = C_c \times (T_c - T_a) \quad (6)$$

Where T_c is the combustion, K. The effectiveness of the hot air exhauster neglecting the effect of temperature on specific heat capacity is then obtain using equation (7) (Çengel et al, 2022):

$$\varepsilon = \frac{C_i(T_e - T_a)}{C_o(T_c - T_a)} \quad (7)$$

Defining the capacity ratio as equation (8):

$$C = \frac{C_i}{C_o} \quad (8)$$

The Number of Transfer Units (NTU) for a multi pass heat exchanger is obtain using equation (9) (Çengel et al, 2022):

$$NTU_m = \left(\frac{-1}{\sqrt{(1+C^2}}\right)\left(\ln\left(\frac{\frac{2}{\varepsilon}-1-C-\sqrt{1+C^2}}{\frac{2}{\varepsilon}-1-C+\sqrt{1+C^2}}\right)\right) \quad (9)$$

The heat transfer area of a multi-pass heat exchanger is obtain using equation (10):

$$A_{sm} = NTU_m \times \frac{C_i}{U} \quad (10)$$

Where U is the overall heat transfer coefficient, $kWm^{-2}K^{-1}$. The perimeter of each pass is given as equation (11):

$$p = 2 \times (w_s + h_x) \quad (11)$$

Where w_s is the width of the hot air exhauster, m, h_x is the height of the hot air exhauster, m. The total length of air passes is obtain using equation (12):

$$L_m = \frac{A_{sm}}{n_p \times p} \quad (12)$$

The total convective area of the hot air exhauster is defining by equation (13):

$$A = L_m \times n_p \times p \quad (13)$$

Where n_p is the number of passes, p is the perimeter of each pass, m.

2.3. Hot Side Heat Exchanger

The hot side heat exchanger has the same architecture as the hot air exhauster. The length and width of the hot side heat exchanger is prefixed with the assembled modules dimension and allowance for coupling. It has a total of four passes to enable the modules absorb maximum heat from the air with a designed inlet air temperature of 100°C, the air exhaust to the atmosphere through an exit pipe. The constructional details of the hot side heat exchanger is as

shown in Fig. 4. The heat input to the generator modules can readily be obtained from equation (14):

$$Q_h = \dot{m}_o C_a (T_{hs} - T_1) \quad (14)$$

Where $\dot{m}_o$ is the mass flow rate of outlet air, kgs^{-1}; C_a specific heat capacity of outlet air, kJkg^{-1}K^{-1}; T_{hs} is the hot side temperature, K; T_1 is the exit temperature of the heat exchanger, K.

2.4. Cold Side Heat Sink

The cold side heat sink is used to absorb and dissipate heat from the thermoelectric modules (Mjallal et al, 2017). The length and width of the heat sink is fixed by the dimension of the sixteen modules assembly with some allowance for coupling the cold and hot side heat exchangers which is fixed as 170 mm x 170 mm. The model of the heat sink is as shown in Fig. 5.

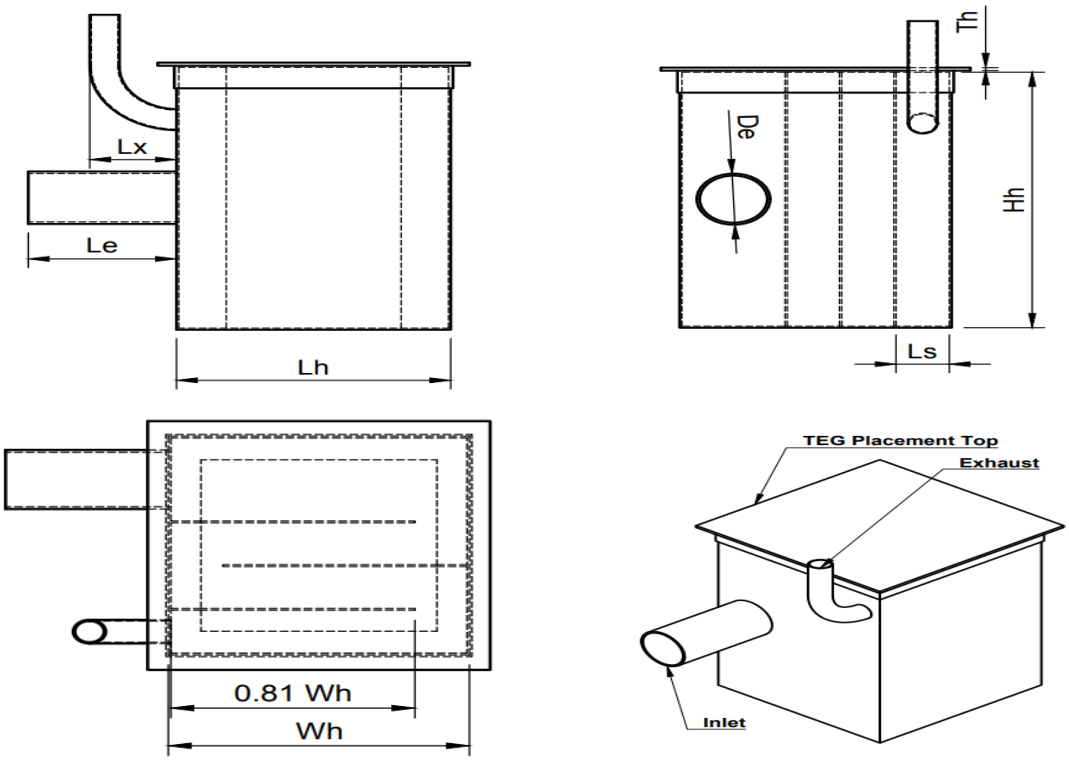

Dimensions in mm: $Lx = 58.56, Lh = 185, Ls = 36.25, Le = 100, De = 50, Hh = 254.5, Wh = 210.4, Th = 3$

Fig. 4. Hot air Heat Exchanger.

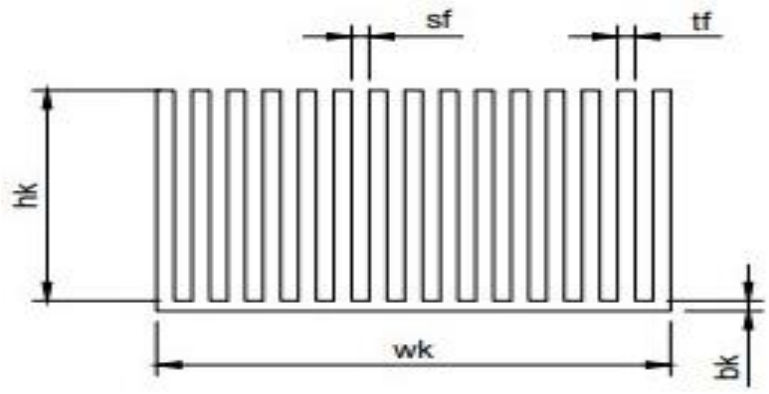

Fig. 5. Cold Side Heat Sink.

Referring to Fig. 5, the base area of the heat sink is expressed as equation (15):

$$A_b = l_k \times w_k \tag{15}$$

Where l_k is the length of heat sink into the paper, m; w_k is the width of heat sink, m. The heat flux is then obtained using equation (16):

$$Q_f = \frac{Q_c}{A_b} \tag{16}$$

Where Q_c is the heat dissipated by the modules, W; A_b is the base area of the heat sink, m^2.

The number of fins is estimated using the width expression defined by relation (17):

$$w_k = \left(n_f \times t_f\right) + (n_f - 1)s_f \tag{17}$$

Yielding

$$n_f = \frac{w_k + s_f}{t_f + s_f} \tag{18}$$

Where n_f is the number of fins; t_f is the fin thickness, m; s_f is the fin spacing, m. The total surface area of the heat sink using Newton's law of cooling is obtained using equation (19) (Reddy, 2015):

$$A_t = \frac{Q_c}{h \times (T_{cs} - T_a)} \tag{19}$$

Where T_{cs} is the cold side temperature, K; h is the heat transfer coefficient, $Wm^{-2}K^{-1}$. The total convective area is given as equation (20):

$$A_t = \left(n_f - 1\right) \times l_k(s_f + 2h_k) \tag{20}$$

From which the height of the fin is obtained using equation (21):

$$h_k = \frac{1}{2}\left[\frac{A_t}{(n_f - 1)l_k} - s_f\right] \tag{21}$$

The base of the heat is estimated using equation (22) (Cengel et al, 2022):

$$t_b = R_\theta k_\theta A_b \tag{22}$$

Where R_θ is the thermal resistance of the base, °C/W; k_θ is the thermal conductivity of heat sink material, $Wm^{-1}K^{-1}$.

2.5. Thermoelectric Generator Performance Indices

Fig. 6 show the SP1848-27145 TEG module consisting of one hundred and twenty six thermocouple junctions under investigation. The module has a dimension of 40 mm x 40 mm x 3.6 mm, a total of sixteen modules was used in the construction in two parallel strings.

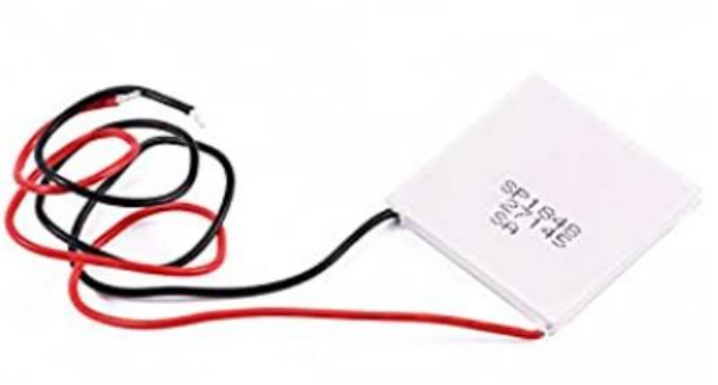

Fig. 6. Thermoelectric Modules.

Energy supplied to the generator is obtained from equation (23) (Nuwayhid et al., 2004):

$$Q_h = nN[2\alpha IT_{hs} + \frac{2kA}{L}\Delta T - \frac{\frac{1}{2}I^2(2\rho L)}{A}] \quad (23)$$

The corresponding energy dissipation from the modules is obtained from equation (24):

$$Q_c = nN[2\alpha IT_{cs} + \frac{2kA}{L}\Delta T - \frac{\frac{1}{2}I^2(2\rho L)}{A}] \quad (24)$$

The net power output for the module arrangement is then obtained from equation (25) (Abubakar et al, 2021):

$$P = nN(Q_h - Q_c) \quad (25)$$

Where ΔT is the temperature gradient, K; Q_h is the heat input supplied to the modules, W ; Q_c is the heat dissipated by the modules, W; N is the number of modules; n = number of couples; A is the area of the thermoelement (leg), m^2 ; L is its length, m; k is the thermal conductivity, $Wm^{-1}K^{-1}$; α is the Seebeck coefficient, μVK^{-1}; ρ is the electrical resistivity, Ωm; I is the electrical current, A. It has been assumed that the Seebeck coefficient, the thermal conductivity and the electrical resistivity of the n and p legs are approximately the same. The open circuit voltage is given by equation (26) (Nuwayhid et al., 2004; Tervo et al, 2009):

$$V_{0c} = 2\alpha nN\Delta T \quad (26)$$

The Voltage at Maximum Power is then expressed a equation (27):

$$V_{mpn} = \frac{V_{oc}}{2} \quad (27)$$

Efficiency of the thermoelectric module is obtained as equation (28):

$$\eta_m = \frac{P}{Q_h} \quad (28)$$

3. METHODOLOGY

This research focused on the design, construction and experimental testing of a hot air thermoelectric generator. The hot air thermoelectric generator consists of the hot side heat exchanger, heat sink with cooling fans, hot air exhauster with attached air blower, dual combustion chamber, battery bank and a charge controller. The components are modeled, sized and simulated using ANSYS Fluent to visualize their thermal performance followed by experimental testing using biomass as source of fuel. Temperatures were monitored with an MTM-380SD temperature data logger, voltage and current were recorded using a multi-meter and air flow rate monitored with a digital GM-8908 anemometer. The experimental setup is as shown in Fig. 7.

Thermoelectric Generator

MTM-380SD Temp. logger

GM-8908 Anenometer

Multimeter

Charge Controller

Fig. 7. Experimental Setup

4. RESULTS AND DISCUSSION

4.1. Computational Fluid Dynamics Analysis of Combustion Hot Air Exhauster

The 3D model of the Combustion Hot Air Exhauster was drawn using Fusion 360 and the simulation was carried out using ANSYS Fluent to depict the temperature profile across the walls and fins of the exhauster. The base plate of the exhauster is maintained at a combustion temperature of 1226°C, air inlet speed of 5.5 m/s and turbulent flow condition, using an

element size of 0.0035, number of nodes 1,046,727, number of elements 726,267 and a convergence criteria of 10^{-4}, the thermograph of Fig. 8 was obtained. Fig. 8 represent the temperature distribution across walls and air channel to which the ambient air incoming is exposed. The maximum experimental recorded air temperature exiting the exhauster is 178.3°C with an effectiveness of 0.17, the lower temperature could be attributed to heat transfer losses in the wall of the exhauster and irregular combustion of the biomass.

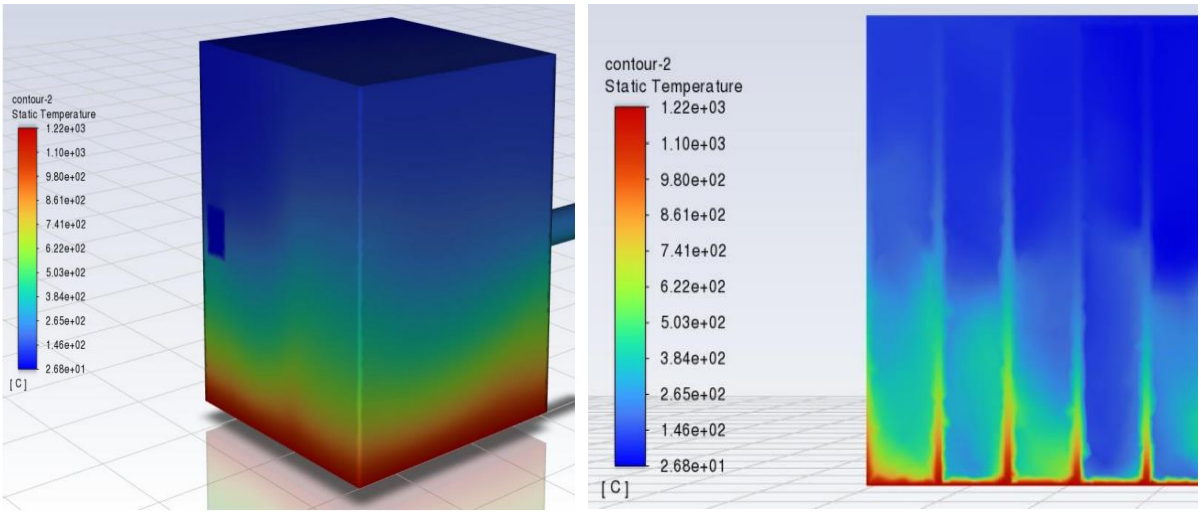

Fig. 8. Thermograph of Hot Air Exhauster.

4.2. Computational Fluid Dynamics Analysis of Hot Side Heat Exchanger

The 3D model of the hot side heat exchanger was drawn using Fusion 360 and the simulation was carried using ANSYS Fluent. The goal of the simulation was to determine the possible outlet air temperature of the heat exchanger and the temperature distribution in the walls and fins of the heat exchanger. The air entering the heat exchanger is maintained at a temperature of 178°C, air inlet speed of 5.5 m/s and turbulent flow condition, using an element size of 0.003, number of nodes 268811, number of elements 1498668 and a convergence criteria of 10^{-3}, the thermograph of Fig. 9 was obtained depicting the temperature to which the thermoelectric modules will be exposed. The maximum temperature at the top of the heat exchanger to which the modules are exposed is 153°C, maximum experimental exit air temperature is 64.2°C, implying that much about of energy is absorbed by the thermoelectric modules in the course of its operation.

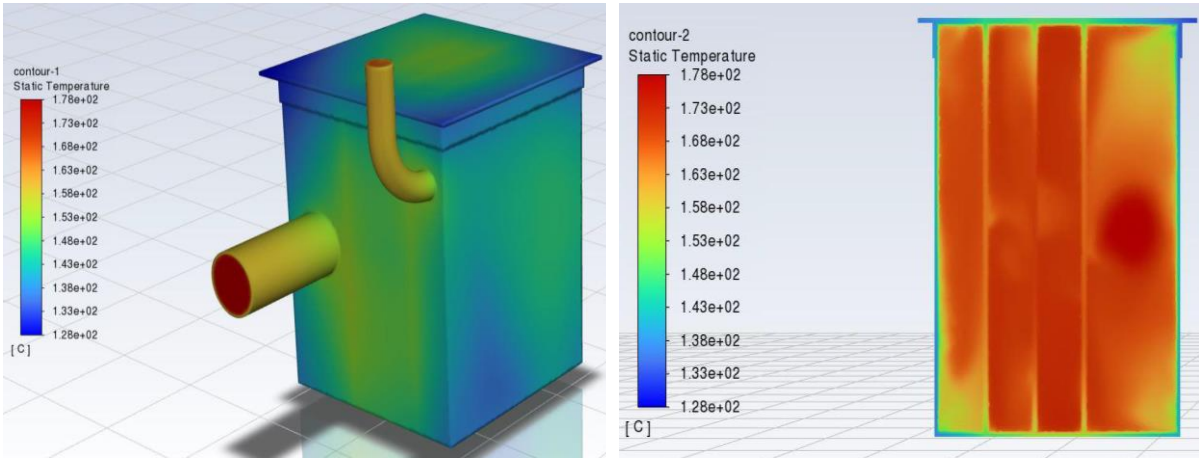

Fig. 9. Thermograph of Hot Air Heat Exchanger

4.3. Computational Fluid Dynamics Analysis of Cold Side Heat Sink

The 3D model of the Heat sink was drawn using Fusion360 and the simulation was also carried using fusion 360's thermal simulation feature. The objective of the simulation is to ascertain the thermal response of the modelled cold side heat sink. Grid dependency test was carried out using a convergence criteria of 0.001, the element size was 1.55 mm, number of nodes was 406340 and the number of elements was 343023. The maximum temperature of the heat sink base and fin tip are 49°C and 45°C respectively, maximum experimental recorded temperature is 44.5°C. The thermograph is a shown in Fig. 10.

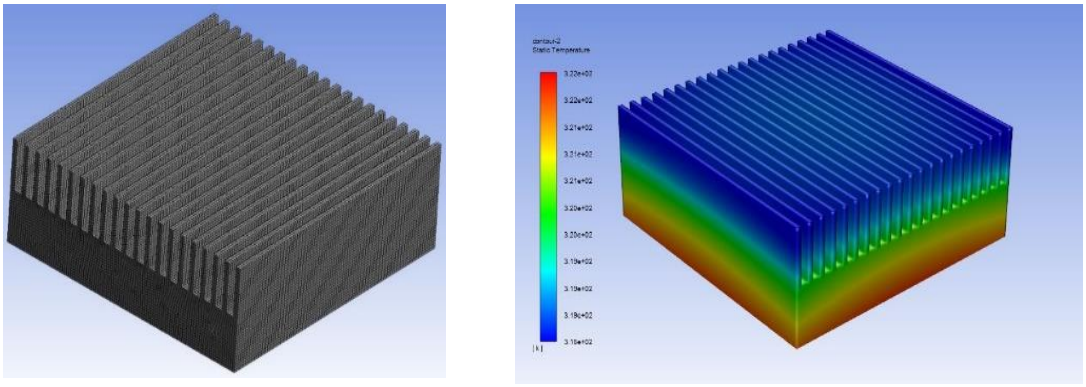

Fig. 10. Temperature gradient for the heat sink simulation

4.4. Thermoelectric Performance Matrices Simulation

Fig. 11 shows a response surface plot for heat supplied to the modules. The plot was generated for different values of hot and cold side temperatures. The optimum values of heat supply exist around the areas where there is low cold side and high hot side values of temperatures.

Fig. 12 shows the surface plot of dissipated heat from the thermoelectric modules also at various hot and cold side temperatures. Clearly heat dissipated is proportional to the temperature gradient across the thermoelectric modules surface.

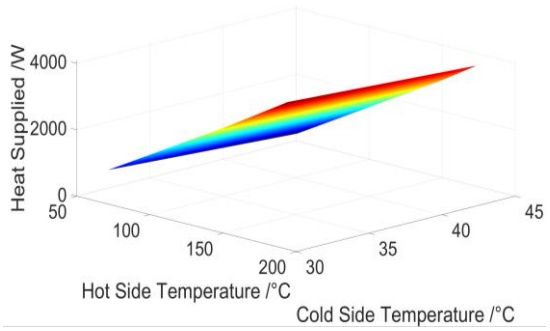

Fig. 11. Heat Supplied vs Hot and Cold side Temperature.

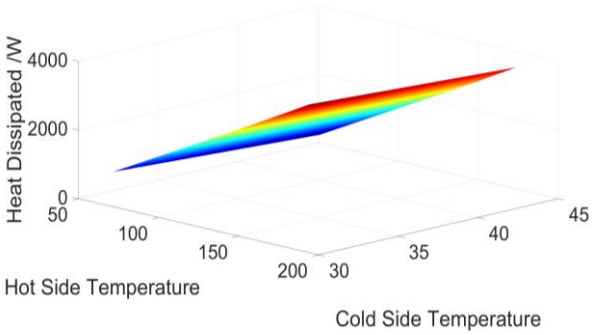

Fig. 12. Heat Dissipated vs Hot and Cold side Temperature.

Fig. 13 shows a response surface plot of the power output of the thermo-electric generator at different values of hot side and cold side temperature. Clearly the power output is directly proportional to the temperature difference the thermoelectric modules are exposed.

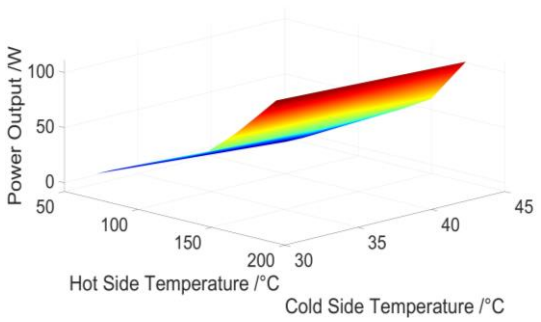

Fig. 13. Power Output vs Hot and Cold side Temperature.

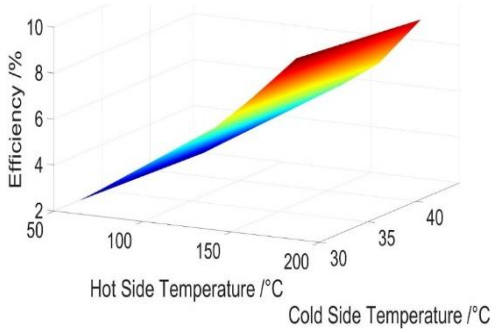

Fig. 14. Efficiency vs Hot and Cold side Temperature.

Fig. 14 shows a response surface plot of the efficiency of energy conversion in the thermoelectric generator at different values of hot and cold side temperatures. Clearly the efficiency of energy conversion is directly proportional to the temperature difference across the exposed surface of the modules. From the simulation, temperature gradient play a significant effect on the performance of the thermoelectric generator.

4.5. Experimental Open Circuit Voltage and Current of the Thermoelectric Generator

Fig. 15 shows the plot of voltage and current against difference in temperature between the hot and cold sides of the thermo-electric modules. The open circuit voltage and current can be seen to increase steadily with an increase in temperature gradient as expected. A maximum voltage of 64 V was recorded at a temperature difference of 133.8°C and at about 150 minutes into the experiment. The corresponding current value at this voltage is 1.99 A.

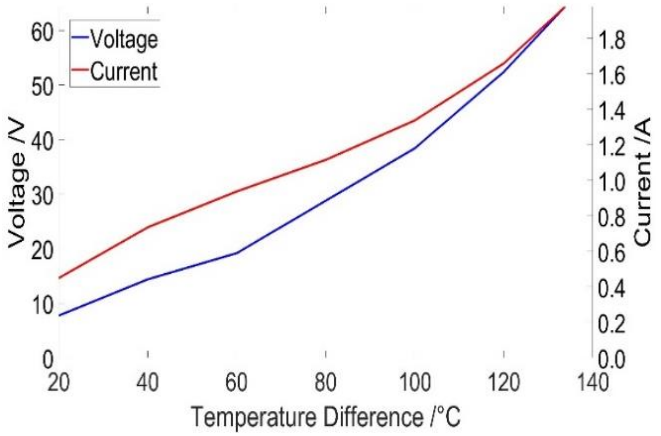

Fig. 15. Voltage and Current vs. Temperature Difference.

5. CONCLUSIONS

Thermoelectric generators are solid-state devices that convert heat into electricity using the Seebeck effect, a phenomenon that causes voltage generation when there is a temperature difference across a thermoelectric material. Thus a model of a thermoelectric hot air generator was designed and experimentally tested using biomass as a heating source. Parameters such as voltage, current and temperatures in the combustion chamber, hot air heat exhauster, hot side heat exchanger and cold side heat sink were measured. The hot air exhauster, hot side heat sink and cold side maximum air temperatures are 178.3°C, 69.2°C and 44.5°C respectively. The thermal performance of the designed hot air exhauster, hot side heat exchanger and cold side heat were simulated using ANSYS Fluent. The maximum open circuit voltage and current recorded during the experiment are 64 V and 1.99 A respectively at a temperature gradient of 133.8°C. Thus, the hot air thermoelectric generator be deployed in off grid centers, rural communities and even in city centers due to high cost of electricity tariffs and rising cost of petroleum products as energy source in internal combustion engine electrical generators.

6. REFERENCES

Abubakar S. U., Jumaat S. A., Akmal J. M. Jamaludin W. A. W. (2021). ‘Analysis of the Performance of Thermoelectric Generators for Ambient Energy Generation through ANSYS Software’. Proceedings of the 11th Annual International Conference on Industrial Engineering and Operations Management Singapore, pp. 3460-3472.

Binu D., Gayathri R., Anand V., Lavanya R., Kanmani R, (2017). ‘Thermoelectric Power Generation Using Solar Energy’. International Journal for Scientific Research & Development, 5(3), pp. 2321-0613.

Bridge B. A., Adhikari D., Fontenla M, (2016). 'Electricity, income, and quality of life'. The Social Science Journal, 53, pp 33 -39.

Çengel, Y. A., Cimbala, J. M., Ghajar, A. J, (2022). Fundamentals of thermal-fluid sciences, 6th Edition, New York, NY: McGraw Hill, chapter 22, pp. 819–839.

Mjallal I., Farhat H., Hammoud M., Ali S., Shaer A.A., Assi A, (2018). 'Cooling Performance of Heat Sinks Used in Electronic Devices'. MATEC Web of Conferences 171, 02003, pp 1 - 4.

Nimankar S. J., Dahake S. K., (2016). 'Review of Heat Exchangers'. Global Journal of Engineering Science and Researches, 3(12), pp 81 - 92.

Nuwayhid R. Y., Shihadeh A., Ghaddar N. (2004). 'Development and testing of a domestic woodstove thermoelectric generator with natural convection cooling'. Energy Conversion and Management, 46, pp 1631 - 1643.

Ong K. S. (2016). 'Review of solar, heat pipe and thermoelectric hybrid systems of power generation and heating'. International Journal of Low-Carbon Technologies, 11(4), pp. 460-465.

Reddy M. C. S. (2015). 'Thermal Analysis of a Heat Sink for Electronics Cooling'. International Journal of Mechanical Engineering and Technology, 6(11), pp 145 - 153.

Remeli M. F., Kiatbodin L., Singh B., Verojporn K., Date A., Akbarzadeh A. (2015). 'Power generation from waste heat using Heat Pipe and Thermoelectric Generator'. Energy Procedia 75, 7th International Conference on Applied Energy, pp. 645 – 650.

Reyes-León A., Velázquez M. T., Quinto-Diez P., Sánchez-Silva F., Abugaber-Francis J., Reséndiz-Rosas C. (2011). 'The Design of Heat Exchangers'. Engineering, 3(9), pp. 911–920.

Saraswathi K. (2020). 'A Review Paper on Electricity Generation from Solar Energy'. International Journal of Scientific Development and Research, 5(4), pp. 279 -284.

Stern D. I., Bruke P. J., Bruns, S. B. (2019). The Impact of Electricity on Economic Development: A Macroeconomic Perspective. Energy and Economic Growth. Applied Research Programme, Paper No: 1.1, pp 1- 42.

Shaikh M. R. S., Waghmare S. B., Labada S. S., Fuke P. J., Tekale A. (2017). 'A Review Paper on Electricity Generation from Solar Energy'. International Journal for Research in Applied Science & Engineering Technology, 5(9), pp. 1884 - 1889.

Stecanella P. A. J., Faria M. A. A., Domingues E. G., Gomes P. H. G., Calixto W. P., Alves A. J. (2015). 'Electricity Generation Using Thermoelectric Generator'. IEEE, 978-1-4799-7993-6/15, pp. 1-5.

Tervo J., Manninen A. J., Ilola R., Hanninen H. (2009). 'State of the Art of Thermoelectric Materials Processing'. Ju lkaisija-Utgivare Publisher, Finland. pp. 1-29.

Virjoghe E. O., Enescu D., Ionel M., Stan M. F, (2018). 'Numerical simulation of thermoelectric system'. Latest Trends on Systems, volume II, pp. 630-635.

Wang J., Li H. (2021). 'The Impact of Electricity Price on Power-Generation Structure: Evidence from China'. Frontiers in Environmental Science, 9, pp 1-10.

Zhu N., Matsuurab T., Suzukib R., Tsuchiyaa T. (2014). 'Development of a Small Solar Power Generation System based on Thermoelectric Generator'. Energy Procedia, 25, pp. 651-658.

Zohuri B. (2016). 'Electricity, an Essential Necessity in our Life, available: https://doi.org/10.1007/978-3-319-23537-0_2, https://www.researchgate.net/publication/301260940 [assessed 5 July, 2023].

Zoui M. A., Bentouba S., Stocholm J. G., Bourouis M. (2020). 'A Review on Thermoelectric Generators: Progress and Applications'. Energies 13(14), pp. 1 - 32.